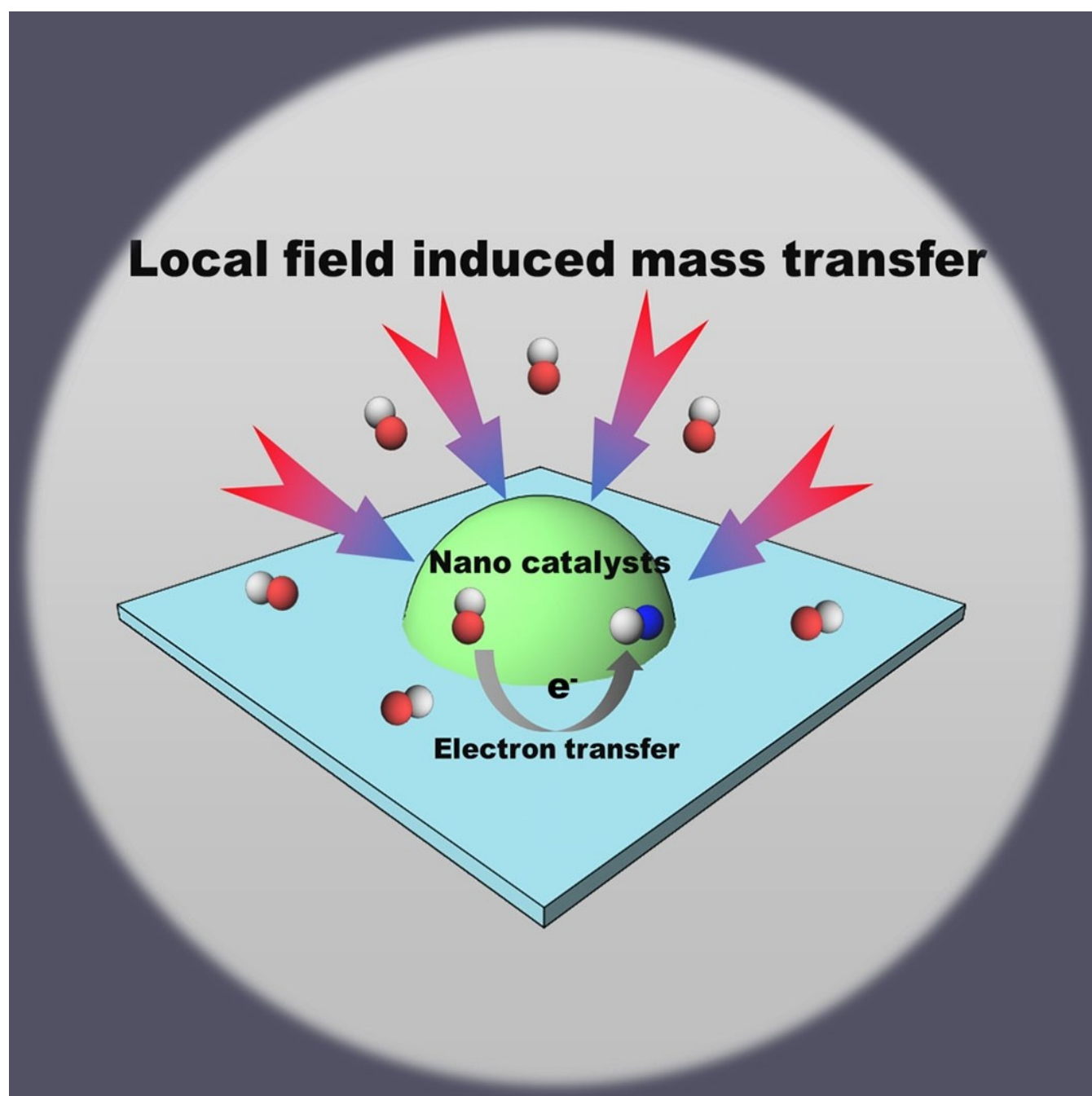


Local Field Induced Mass Transfer: New Insight into Nano-electrocatalysis

Yinghuan Liu,^[b] Huijun Jiang,^{*[a, b]} and Zhonghuai Hou^[a, b]



Abstract: Unravelling the complex kinetics of electrocatalysis is essential for the design of electrocatalysts with high performance. Mass transfer and electron transfer are two primary factors that need to be optimized in order to enhance electrocatalytic reactions. The use of nanocatalysts proves to be a promising way of promoting the performance of electrocatalytic reactions, this improvement is usually attributed to their ability to enhance electron transfer. However, when catalysts are taken down to the nanoscale, their size is

comparable to the thickness of an electrical double layer, so any curvature can lead to an inhomogeneous local electric field on the electrode, which then changes the mass transfer essentially. In this article, we introduce the new concept of local-field-induced mass transfer in nano-electrocatalytic systems, and provide a brief review of recent progress, revealing its effect on nano-electrocatalysis, which may bring new insight into the future design of nano-electrocatalysts.

Introduction

Over the past decades, increasing energy demands and the growing green-house effect have become major problems in society.^[1–4] One promising solution to these problems is developing electrocatalytic processes that could convert easily obtained raw materials such as CO₂ and N₂ in the atmosphere into high-value products such as hydrocarbons and ammonias with renewable energy.^[5–6] Specially, electrochemical reactions such as CO₂ reduction would reduce the green-house effect by capturing CO₂ in the atmosphere, close the carbon cycle, and transform renewable energy into high-energy-density and more stable liquid fuels.^[3,7–9] Understanding the complex electrocatalytic process would be essential for the rational design of electrocatalysts with desired activity and selectivity. Mass transfer and electron transfer are two primary factors need to be optimized in order to enhance electrode reaction.^[10,11] Mass transfer for electrocatalysis may include diffusion or migration of chemical species along the normal direction of the electrode surface, which can be accelerated by rotating disk electrode or stirring the solution.^[10,12–15] In the meanwhile, electron transfer can be enhanced by promoting the intrinsic activity by regulating electronic structure of the catalyst or increasing active sites by splitting the catalyst into small parts.^[16–19]

A promising way increasing both the intrinsic activity and the number of active sites is to take the catalyst down to the nanoscale.^[20–22] For example, cubic Pt nanocrystal obtains a three folds increasing in benzene hydrogenation rate,^[23] tetrahexahedron Pt nanocrystal is three times more efficient for the electro-oxidation of ethanol and up to 200% more efficient for formic acid electro-oxidation as comparing with conventional bulk Pt catalyst,^[23] and copper nanowire with rich surface steps exhibits a remarkably high Faradaic efficiency for C₂H₄.^[24]

Besides electron transfer, there is some evidence implying that mass transfer might also differ from that predicted by conventional theories for nanocatalysts.^[25–29] An essential difference is that the thickness of electrical double layer is comparable to the size of the nanocatalyst, so that curvatures of the catalyst at nanoscale lead to inhomogeneous local electric field on the electrode.^[30–35] Consequently, such local electric field would induce mass transfer along directions paralleling to the electrode surface, which is absent in conventional theories.

In this concept, we provide a brief review of several recent progresses revealing the effect of local-field-induced mass transfer (LMT) on nano-electrocatalysis, and highlight the new insight of LMT in future design of nano-electrocatalysts. In the first part, a general model for electrocatalysis is introduced. After that, a theoretical framework is established to describe comprehensively the kinetic process of nano-electrocatalysis with LMT. In the third part, the proposed theoretical framework is applied to several nano-electrocatalytic systems to reveal their underlying mechanisms, where LMT is found to play an important role in enhancement of both reaction activity and selectivity.

General Model for Electrocatalysis


In general, the whole process of heterogeneous electrocatalytic reactions include mass transfer from bulk solution to the electrode surface, electrochemical reaction on electrode surface (electron transfer), and other chemical reactions as shown in Figure 1a.^[10] Electron transfer and mass transfer are primary factors for electrode reactions and the interplay between them governs the voltammetry behaviour of electrode reaction as shown in Figure 1b.^[34] This section briefly reviews conventional models and theories of electron and mass transfer.

Electron transfer

There are two representative models to describe the electron transfer process, that is, Butler-Volmer (BV) model and Marcus-Hush-Chidsey (MHC) model.^[36–39] For a simple reaction involving one transferred electron, Red + e[−] = Ox, the net reaction rate of electrocatalytic reaction on the electrode surface is $v_{\text{net}} = k_{\text{Re}}c_{\text{Re}} - k_{\text{Ox}}c_{\text{Ox}}$, where k_{Re} and k_{Ox} are the oxidation and reduction

[a] Dr. H. Jiang, Prof. Z. Hou
Hefei National Laboratory for Physical Sciences at the Microscale
University of Science and Technology of China
230026, Hefei (P. R. China)
E-mail: hjjiang3@ustc.edu.cn

[b] Y. Liu, Dr. H. Jiang, Prof. Z. Hou
Department of Chemical Physics, iChEM
University of Science and Technology of China
230026, Hefei (P. R. China)

 Selected by the Editorial Office for our Showcase of outstanding Review-type articles <http://www.chemeurj.org/showcase>.

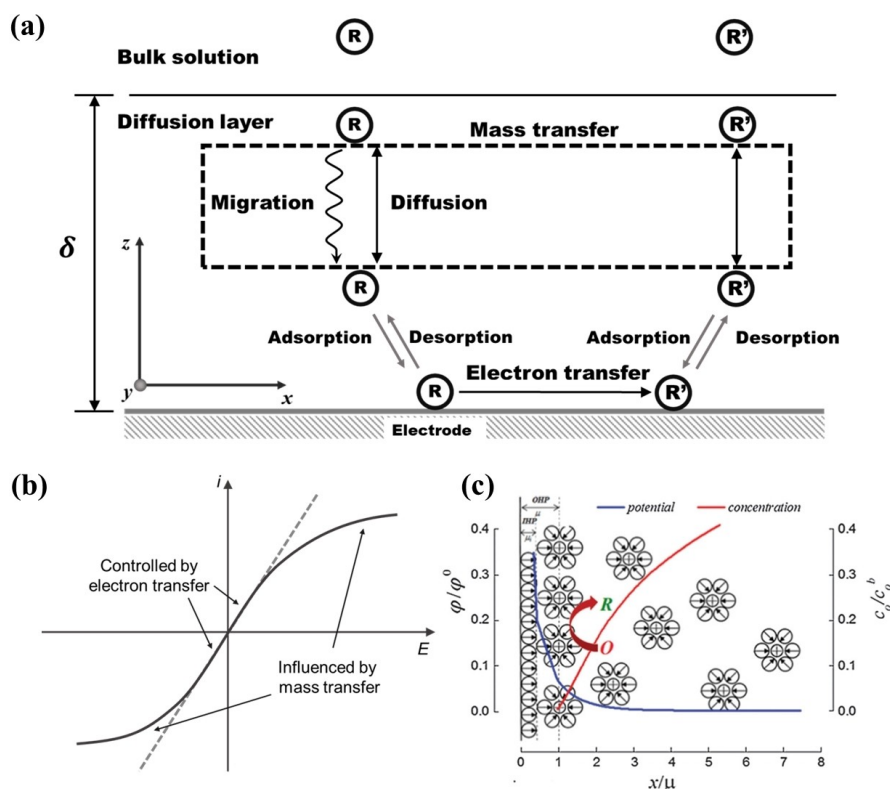


Figure 1. Schematic of a) the overall kinetics for electrocatalysis, b) current–potential curve and c) the structure of an electrode/electrolyte interface for electrochemical reactions. The dashed line in (b) is for ideal electrodes, while the solid line is for real electrodes. The blue and red solid lines in (c) illustrate the distributions of the electrostatic potential and the concentration of the reactant, respectively. (Figure adapted with permissions from ref. [35]. Copyright: 2014, The Royal Society of Chemistry.)

reaction rate constants, c_{re} and c_{ox} are the concentrations of reduction and oxidation species, respectively. BV model indicates the relationship between overpotential and reaction rates constant as $k_{\text{re}} = k^0 \exp\left(\frac{-\alpha F \eta}{RT}\right)$ and $k_{\text{ox}} = k^0 \exp\left(\frac{(1-\alpha) F \eta}{RT}\right)$, where k^0 is the standard rate constant, α is the transfer coefficient, F is the Faraday constant, R is the gas constant, T is the temperature, and $\eta = E - E_0$ is the overpotential with E being the applied potential and E_0 the formal potential.^[38] The current-potential characteristic thus can be derived as $i = FAk^0 [C_{\text{O}}(0, t) \exp\left(\frac{-\alpha F \eta}{RT}\right) - C_{\text{R}}(0, t) \exp\left(\frac{(1-\alpha) F \eta}{RT}\right)]$, where A is frequency factor and $C_{\text{O(R)}}(0, t)$ is the surface concentration of oxidation (reduction) species at time t . For reactions limited by the solvent and/or ligand reorganization, MHC model further considers the effect of solvent and/or ligand on electrocatalytic reactions, where the reaction rate constants read

$$\frac{k_{\text{Re/Ox}}^*}{k_0^*} = \frac{\int_{-\infty}^{+\infty} \frac{1}{1 + \exp(\frac{\eta}{\lambda})} \exp(-\Delta G_{\text{Re/Ox}}^*) d\epsilon^*}{\int_{-\infty}^{+\infty} \frac{1}{1 + \exp(\frac{\eta}{\lambda})} \exp(-\Delta G_{\text{Re/Ox}}^*) (\eta^* = 0) d\epsilon^*} \quad \text{and}$$

$$\Delta G_{\text{Re/Ox}}^* = \frac{\lambda^*}{4} \left(1 \mp \frac{\eta^* + \epsilon^*}{2}\right)^2, \quad \text{where } \lambda \text{ is the reorganization energy which actually reflects the hindrance of the electron transfer, and } \epsilon \text{ is the energy level } \lambda, \epsilon \text{ and } \eta \text{ with superscript } * \text{ are their dimensionless form with the unit } F/(RT). k_0^* \text{ is } k_0^* \text{'s dimensionless form with the unit } r/D.$$

Mass transfer

As shown in Figure 1b, the overall reaction kinetics is dominated by the electron transfer under low current density and low overpotential. However, for high current density, mass transfer would also influence the overall kinetics by limiting concentration of reactants near the electrode surface.^[40]

For catalysts in macroscale, the mass transfer is usually considered to be along the normal direction of the electrode surface (z direction in Figure 1a). A Nernst–Planck equation would quantify the mass transfer of species i as $J_i(z) = -D_i \frac{\partial C_i(z)}{\partial z} - \frac{n_i F}{RT} D_i C_i \frac{\partial \phi(z)}{\partial z} + C_i v(z)$. The first term in the right side is the diffusion of species i along the gradient of concentration according to Fick's law with D_i the diffusion constant and C_i the concentration. The second term is the migration of species i , that is, directional mass transfer induced by the electric field near the electrode surface,^[41] where n_i is the charge of species i and $\phi(z)$ is the potential distribution. An electrical double layer (EDL) model is applied to describe the potential distribution in electrode–solution interface (Figure 1c). In this model, EDL is composed of a compact layer and a diffuse layer. The compact layer is composed of inner Helmholtz plane (IHP) and outer Helmholtz plane (OHP). The solvent molecular and species which are specifically adsorbed on the electrode surface are located in inner Helmholtz plane. The diffuse layer is ranges from inner layer to bulk solution.^[42] The last term is the

convection term. $v(z) = ku(z)$ is the magnitudes of the solution velocities in the direction of z , where \mathbf{k} is the unit vector and $u(z)$.

Overall kinetics for electrocatalysis at the macroscale

The above electron transfer and mass transfer govern the overall kinetics of electrocatalysis at the macroscale. Coupling of the two processes leads to a concentration gradient from bulk solution to electrode surface. This concentration gradient can be described by a diffusion layer with the thickness of δ near the electrode surface as shown in Figure 1a. The thickness of the diffusion layer can be greatly reduced by high stirring rates or the utilization of rotating disk electrode. Within the diffusion layer ($0 \leq z \leq \delta$), diffusion and migration along the z direction contribute to the mass transfer. On the electrode surface ($z=0$), electron transfer model described in *Electron transfer* section can be set as a boundary condition. After performing Nernst–Planck equation with the above boundary conditions in the z direction, the concentration distribution of species i in the diffusion layer and on the electrode surface, $c_{\text{Re(Ox)}_i}$ can be obtained.

Theoretical Framework for Nano-electrocatalysis with Local Fields

This section reviews a theoretical frame established to describe comprehensively the kinetic process of nano-electrocatalysis with inhomogeneous local electric field. One of the distinctions between electrocatalysis on macroscale catalysts and nanocatalysts is the distribution of electric field near surface. EDL is applied to describe the distribution of electric field and its induced electrical potential near the catalysts surface. When the concentration of electrolyte changes from 1.0 to 10^{-5} M, Debye length (characteristic scale of the EDL) would change from 0.1 to 100 nm.^[42] For macrocatalysts, the Debye length is rather small comparing with the size of catalysts and thus conventional theories treat EDL as planer layers over macrocatalysts surface as shown in the upper schematic of Figure 2a. For nanocatalysts, sizes of catalysts are comparable to the Debye length and lead to curved EDL layers over nanocatalysts as shown in the lower schematic of Figure 2a.^[41] The gradient of electrical potential on macrocatalysts is thought to be along the z direction (normal direction of the electrode) and correspondingly leads to a conventional mass transfer in the z direction. For nanocatalysts, however, the gradient of electrical potential would not only along the z direction but also along the x and y directions (parallel direction of the electrode) and induce extra mass transfer in the x and y directions (i.e., local electric field induced mass transfer, LMT).

Jiang and his co-workers developed a theoretical framework to unravel the underlying mechanism of kinetics for nano-electrocatalysis with specific consideration of LMT^[43–46] as shown in Figure 2b. Kinetic factors such as effective adsorption/

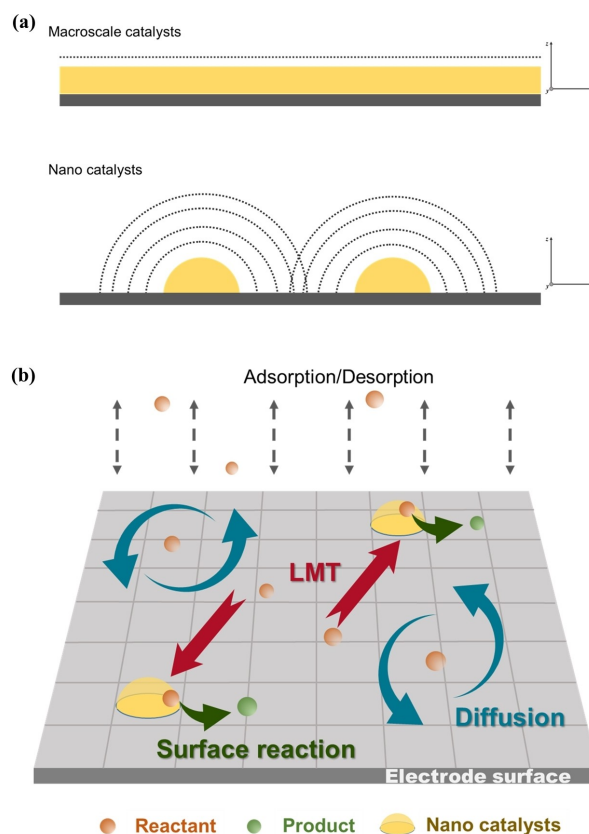


Figure 2. a) Schematic of the electric field induced by a macro electrode (above) and nanocatalysts (below). Dashed lines denote the contour line of electric potential. b) Schematic of the theoretical framework for nano-electrocatalysis.

desorption of reactants from solution to the electrode surface, diffusion, LMT on the surface and electron transfer on nanocatalysts are included in this framework. To obtain dynamics equations describing the overall kinetics, the electrode surface is divided into $N \times N$ grids. Inside these grids, total number of reactant molecules should be large enough so that the relevant thermodynamic quantities, such as the local free energy, can be defined at any moment t . The number, on the other hand, must be small enough so that these quantities can be considered as constant within each grid, and local equilibrium is assumed to hold, that is, inside each grid the thermodynamic potentials have the same form as in equilibrium, but with varying state variables. Electric field distributes on catalysts surface as electrocatalysis takes place. Such electric field would induce movement of ions or polarized molecules or charged complex. An interaction potential of a general form $V(r)$ is used to describe this interaction potential. The motion of molecules in the electric field can statistically expressed by the change of local coverage $\theta_i(r)$. $\theta_i(r)$ governs the rate of chemical reactions on catalysts surface and is a descriptor for state of the studied system with LMT effect. For a grid locating at position r , the system's free energy density functional with a general interaction potential $V(r)$ of chemical species in the local electric field can be written as $f(r) = \sum_i V_i(r) + \sum_i k_B T [\theta_i(r) \ln(\theta_i(r)) +$

$(1 - \theta_i(r)) \ln(1 - \theta_i(r))$], where $\theta_i(r)$ is the effective coverage of species i . Thus, the chemical potential for species i can be derived as $\mu_i(r) = \partial_{\theta_i} V_i(r) + k_B T \ln \frac{\theta_i(r)}{1 - \theta_i(r)}$. Additionally, it is also assumed that the transport process is not far from equilibrium so that the mass transfer flux depends linearly on the corresponding driven force $J_i(r) = -L_i \nabla \mu_i(r) = -L_i [\nabla (\partial_{\theta_i} V_i(r)) - \frac{k_B T}{\theta_i(r)(1 - \theta_i(r))} \nabla \theta_i(r)]$. This flux must be back to Fick's law with the absent of $V(r)$. Then it can be obtained that $L_i = \frac{D_i \theta_i(r)(1 - \theta_i(r))}{k_B T}$. Consequently, we have the mass transfer flux $J_i(r) = -D_i \nabla \theta_i(r) - \frac{D_i}{k_B T} \theta_i(r)(1 - \theta_i(r)) \nabla (\partial_{\theta_i} V_i(r))$. It is assumed here that chemical species are adsorbed on different sites of the surface. If some of the species are adsorbed on the same sites, there should be competition between the adsorption process of them. The $(1 - \theta_i(r))$ term which represents the empty site for i should be replaced by $(1 - \sum_j \theta_j(r))$. Combined with the electron transfer and other related chemical reactions, the reaction-diffusion equation for species i at position r reads

$$\frac{\partial \theta_i}{\partial t} = \sum_{j=1}^M g_j(\{\theta_j\}) + D_i \nabla^2 \theta_i + \frac{D_i}{k_B T} \nabla [\theta_i(r)(1 - \theta_i(r)) \nabla (\partial_{\theta_i} V_i(r))] \quad (1)$$

where g_j stands for the j -th reaction, and M is the total number of reactions.

Applications

Application of the above theoretical framework on a specific nano-electrocatalytic system, the role of LMT and other kinetic factors in overall kinetics of nano-electrocatalysis is ready to be explored.

Curvature effect

Recently, Liu et al. reported experimentally that the curvature of electrode would affect the CO₂ reduction reaction (CO₂RR) on it.^[47,48] The activity of CO₂RR performed on nanocatalysts with needle shape is about two orders of magnitude higher than that on nanoparticles. Faradic efficiency of C products on nanoneedles reaches about 90%. It is shown in Figure 3a that local electric field induced by high curvature catalysts (left) is higher than that induced by medium and low curvature catalysts (medium and right). Jiang et al. then applied the above theoretical framework to perform simulations of CO₂RR on electrode surface with different curvatures. Dependence of the optimal sharp-tip enhanced CO₂RR performance on reaction rate constant k is shown in Figure 3b, where R^* , v^* , and e^* are the tip size, CO producing rate, and efficiency when the optimal performance is achieved for a given k . It can be found that, the optimal performance of CO₂RR is quite robust to the change of the energetic barrier. This simulation result implies that the main reaction, CO₂RR, has already been accelerated enough so that the optimal sharp-tip enhanced performance cannot be

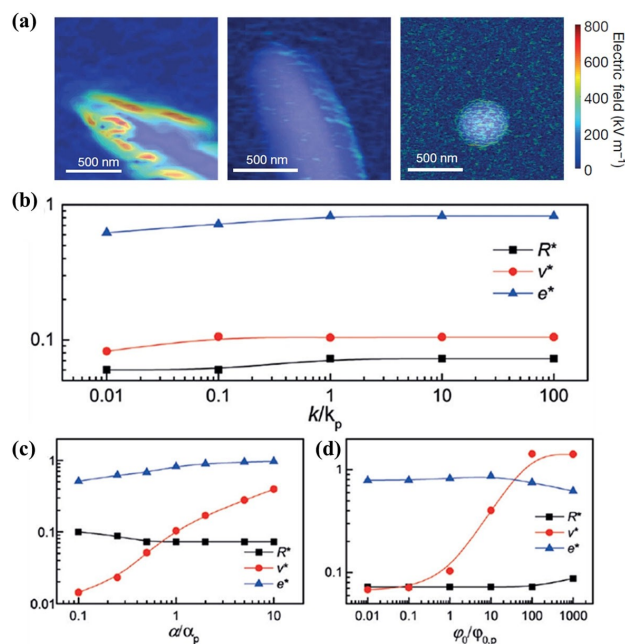


Figure 3. a) Electric field distribution of Au needles, rods and particles. Effect of optimal sharp-tip enhanced CO₂RR performance on b) reaction rate constant k , c) interaction strength between adsorbed CO₂ and the local electric field, and d) effective adsorption rate for CO₂ on the electrode surface. R^* , v^* , and e^* are the tip size, CO producing rate, and efficiency for optimal performance. (Figure adapted with permissions from refs. [43] and [47]. Copyright: 2017: Wiley-VCH and 2016, Macmillan Publishers Ltd.)

further enhanced by simply lowering the energy barrier of the main reaction. Figure 3c shows that the optimal CO₂RR performance depends strongly on the interaction strength between adsorbed CO₂ and the local electric field. Figure 3d shows change of the CO₂RR performance with the effective adsorption rate for CO₂ on the electrode surface. These simulation results demonstrate that when diffusion of CO₂ to the catalysts cannot match the fast reaction, LMT provides extra CO₂ for CO₂RR. This sharp-tip enhanced CO₂RR mechanism implies that LMT plays significant role for enhancing electrocatalytic performance on nanocatalysts.

This mechanism is also verified in other nano-electrocatalytic systems,^[49,50] such as boosting the activity of CO₂ to CO conversion with sharp tipped zinc nanowires,^[51] structuring sharp Cu@Sn nanocones on Cu foam for highly selective electrochemical reduction of CO₂ to formate,^[52] using high curvature transition metal chalcogenide nanostructures for high performance of CO₂RR,^[53] sharp-tip enhanced catalytic CO oxidation by atomically dispersed Pt1/Pt2 on a raised graphene oxide platform,^[54] enhancing CO₂ reduction with polytetrafluoroethylene protected copper nanoneedles^[55] as well as dispersing platinum atomically on curved carbon supports for efficient electrocatalytic hydrogen evolution^[56] and anchoring protrusion-like single atoms on MoS₂ for promotion of N₂ reduction.^[57]

Assembly configuration

Chen and Liu et al. reported that assemble nanocatalysts into ordered nanostructure would enhance electrocatalytic reaction rates.^[44] They applied methanol oxidation reaction (MOR) as an example reaction on orderly aligned Pt nanotubes, and demonstrated that the reaction rates on this nanocatalysts is higher than that on disordered catalysts. Figure 4a describes the configuration of ordered and disordered catalysts. Performance of MOR on ordered and disordered catalysts is shown in Figure 4b, where ordered catalysts deliver a MOR mass activity nearly 2 times higher than the activity on disordered catalysts. The above theoretical framework is then applied to perform MOR on electrode with ordered aligned nanotubes. Figure 4c and d shows the interaction potential of CH₃OH in local electric field induced by ordered and disordered catalysts, respectively. The simulation results show that ordered catalysts would form ordered potential pattern consists of well-arranged valleys as

shown in Figure 4c. The locations of those valleys are corresponding to the locations of ordered nanotubes. For disordered catalyst the well-arranged potential valleys are disappeared and several large potential wells are observed as shown in Figure 4d. Under this configuration, many nanotubes or segments of nanotubes locate at or near the peak of the potential, only few of them locate in the potential wells. Figure 4e and f shows the sectional potential on Pt NTs in ordered and disordered configurations. The results indicate that CH₃OH molecules on ordered catalysts would be transferred to the catalysts from nearby electrode surface along potential gradient, while CH₃OH molecules on disordered catalysts would not be transferred to a large amount of nanotubes not located in the potential wells. As a result, catalysts with ordered configuration would regulate LMT for higher electrocatalytic performance.

This mechanism is also intended to be utilized in other configurations or electrocatalytic systems, such as enhancing

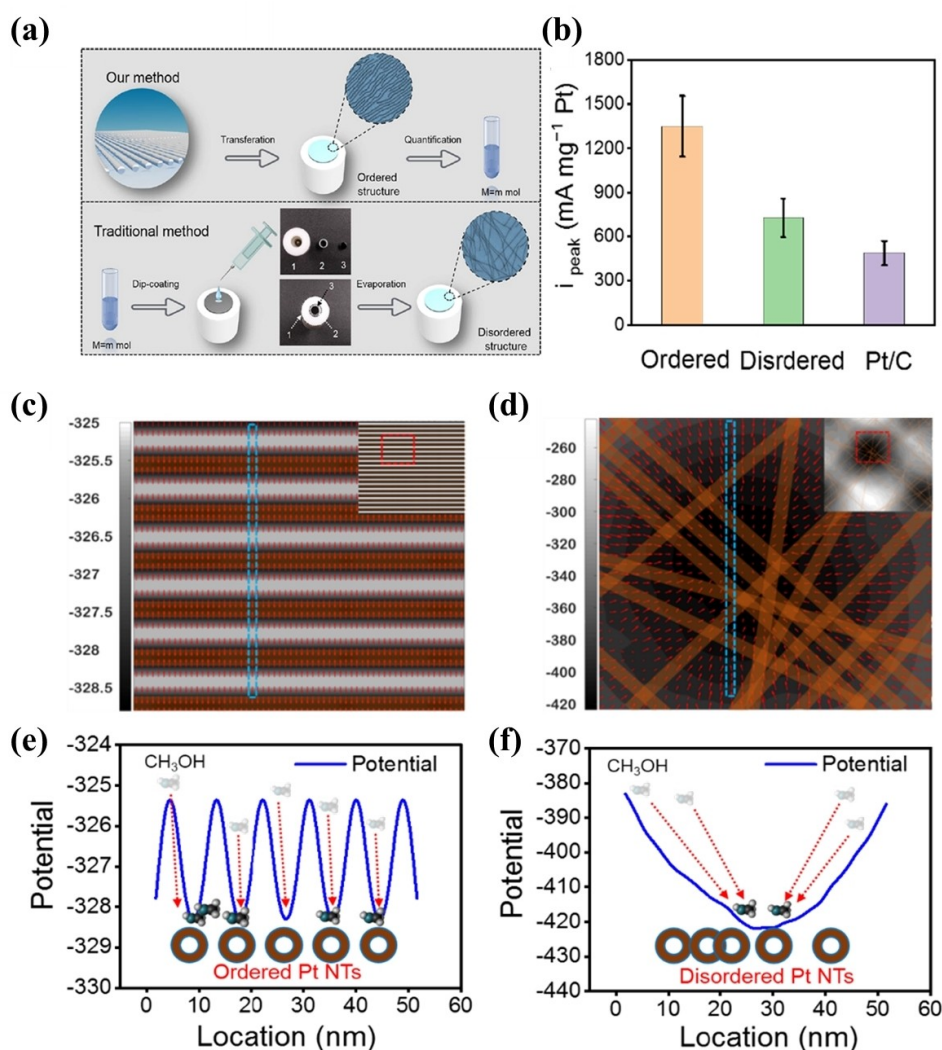


Figure 4. a) Schematic of ordered and disordered Pt NTs catalysts. b) Electrocatalytic performance of different Pt catalysts for MOR. Effective potentials of CH₃OH in local electric fields induced by c) ordered and d) disordered catalysts. Sectional potentials on Pt NTs in e) ordered and f) disordered configurations; red dashed arrows show the mass-transfer direction of CH₃OH. (Figure adapted with permissions from ref. [44]. Copyright: 2019, American Chemical Society.)

ionic conductivity in composite polymer electrolytes with well-aligned ceramic nanowires,^[58] facilitating charge storage at electrified interfaces with self-assembled nanostructures in ionic liquids,^[59] fabricating structurally ordered ionic liquid-layered double hydroxide to amplify chemiluminescence signals,^[60] structuring hollow Palladium-Gold nanochains with periodic concave structures as superior oxygen reduction reaction electrocatalysts and highly efficient surface-enhanced Raman scattering substrates,^[61] assembling of gold nanowires on gold nanostripe arrays for applications in electronic/optic and power storage devices^[62] as well as mechanical design of brush coating technology for the alignment of one-dimension nanomaterials.^[63]

Apart from assembling 1D nano materials in ordered configuration, aligning them into 3D channel also proved to be an efficient way inspiring high electrocatalytic performance.^[64,65] Chen and Liu et al. reported the design of 3D ordered and crosslinked channel (3DOC) for high activity electrocatalytic reaction as shown in Figure 5a.^[45] Figure 5b indicates that the activity of exemplified reaction, MOR, would be largely enhanced

by a 3DOC structure (solid bars) comparing with disordered 1D nano materials (strip bars). 3DOC-M (M = 1/2/3/4) refers to channel sizes of 40, 60, 90, and 120 nm. MOR activity on 3DOC is influenced by the channel size and 3DOC with a channel size of 60 nm exhibits the optimum apparent reaction rate.

The above theoretical framework is then applied to perform MOR on electrode with 3DOC to understand the size effect. Figure 5c and d shows interaction potentials of CH₃OH in the 3DOC with channel sizes of 40 and 120 nm, respectively. Higher overlapped local electric field with lower potential gradient is induced inside small channels than that inside large channels, indicating that LMT in channel with small size is suppressed. This suppressed LMT would lead to lower concentration of CH₃OH on catalysts. Besides LMT, other factors of the nano-channels such as impedance would also influence the MOR activity. Experimental results denote that an increased channel size would lead to an increased impedance for electron transfer. Higher electron transfer impedance leads to a lower reaction rate constant for electron transfer process. The trend of CH₃OH surface concentration on catalysts and reaction rate constant

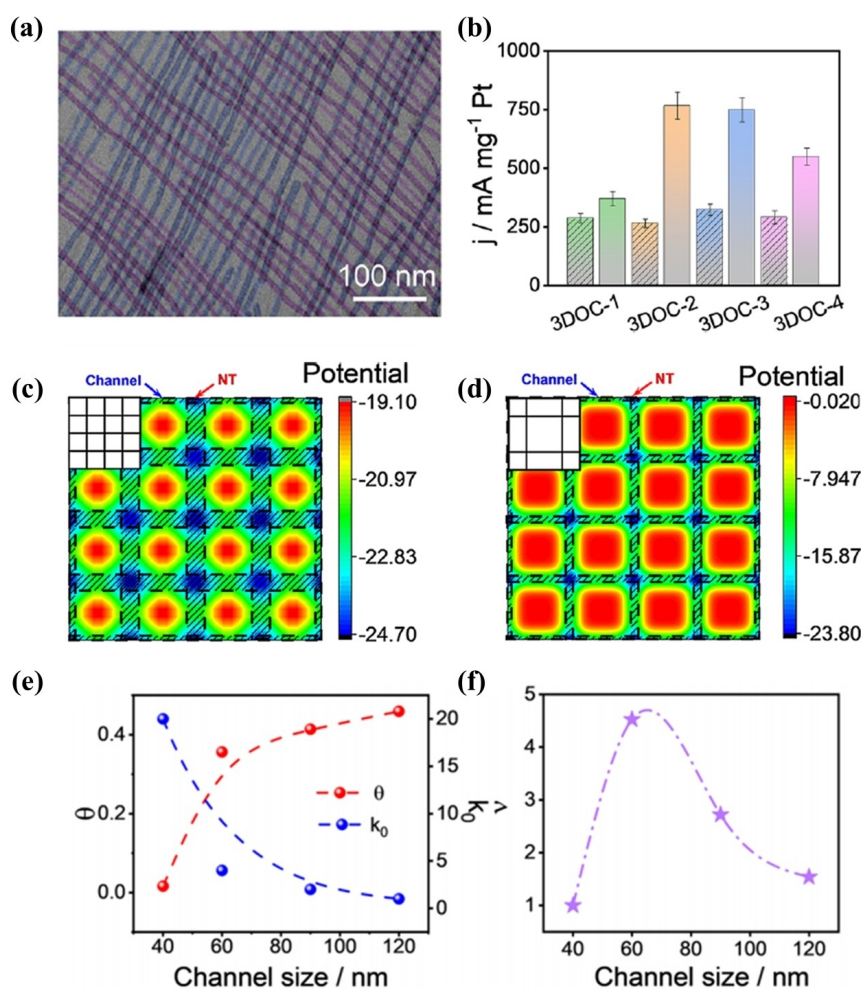


Figure 5. a) TEM image of 3DOC catalysts. b) MOR activity on 3DOC with different sizes (solid bars) and disordered nanotubes (striped bars). Interaction potentials of MeOH in the 3DOC with channel sizes of c) 40 and d) 120 nm. Insets: Schematics of the 3DOC, where the black line represents the positions of catalysts. e) Reaction rate constant (blue) and surface concentration (red) varying with channel size. f) The overall MOR activity changes with the increasing channel size. (Figure adapted with permissions from ref. [45]. Copyright: 2021, American Chemical Society.)

varied with channel size is shown in Figure 5e. The coupling of increased local concentration and decreased reaction rate constant renders a volcano-like reaction rate trend with increasing channel size (Figure 5f). Consequently, a proper channel size for optimized MOR activity would be obtained. This work reveals that LMT and impedance are changed with channel sizes in 3DOC. The interplay between them is a significant kinetic factor for the electrocatalytic performance.

Roughness effect

Recent experiments reported by Jaramillo and his co-workers demonstrated that increasing the roughness of Cu electrodes would promote the selectivity of multi-carbon products in carbon monoxide reduction reaction (CORR) comparing with the competed hydrogen evolution reaction (HER).^[66] After normalized the activity of CORR and HER by electrochemically active surface area, they found that high RF Cu electrodes would suppress the intrinsic activity of HER rather than promote the intrinsic activity of CORR. Since two well-known factors that influence the activity of HER, that is, energy barrier and local pH, failed to understand this roughness led HER suppression

as described in this work, it implies a new mechanism underlying the high roughness enhanced CORR selectivity.

The above theoretical framework is then applied to perform CORR and HER on high roughness catalysts which is mimicked by several high curvature sites (HC sites) on the electrode by Hou and Jiang et al.^[46] The simulation results reproduced the experimental results well and showed that the surface coverages of OH⁻ on electrode surface with different RF are distinct. As shown in Figure 6a, probability distribution of OH⁻ coverage on small RF catalysts ($N=5,10$), medium RF catalysts ($N=20,30$) and high RF catalysts ($N=40$) shows that, increasing RF would lead to a raising OH⁻ coverage on HC sites. The raising of OH⁻ coverage on HC sites then suppresses HER on high RF catalysts. Stationary distribution of θ^{OH} on different electrodes are shown in Figure 6b and c. Overtly, on low roughness catalysts, as shown in Figure 6b, there are several low coverage regions and all of the HC sites locate in the centre of these regions. For high roughness catalysts, most of the HC sites are located in relative high coverage region instead of locating in low coverage region (Figure 6c). Interaction potential between local electric field and OH⁻ on catalysts surface with low RF and high RF are shown in Figure 6d and e, respectively. It can be observed that several separated high potential areas are located near HC sites on electrodes with low RF, resulting in directional LMT from HC

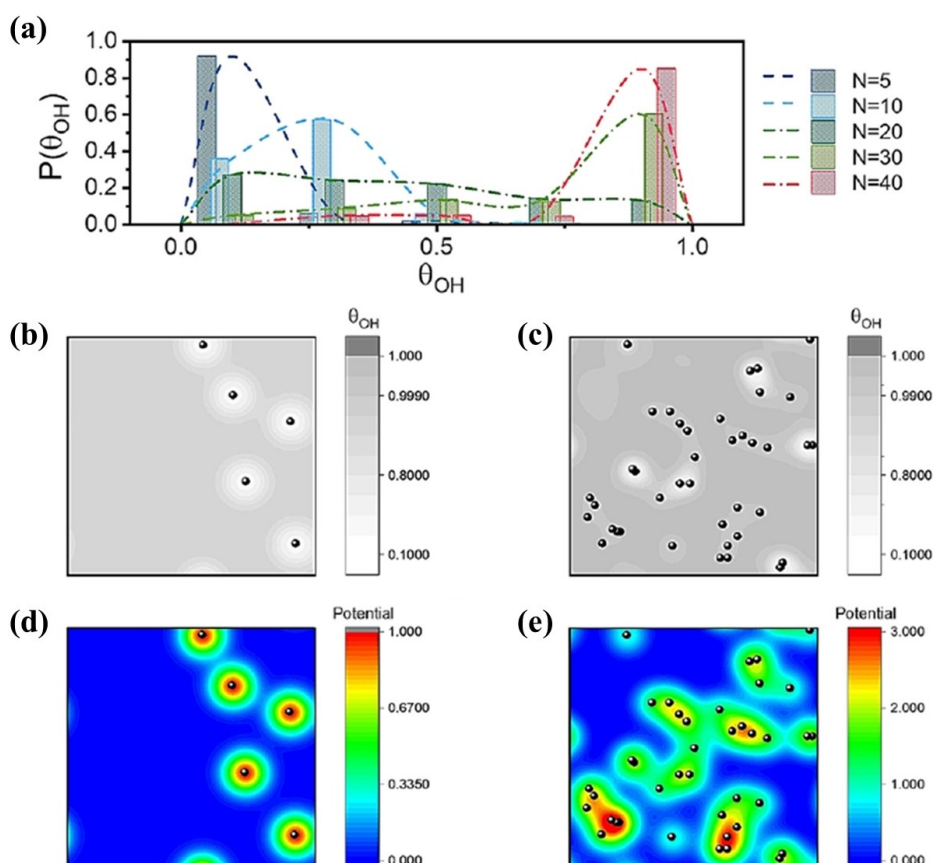


Figure 6. a) Probability distribution of OH⁻ groups on the HC sites of catalysts. Surface coverage of OH⁻ on catalysts with roughness b) $N=5$ and c) $N=40$. Potential of OH⁻ groups in the electric field induced by catalysts with d) $N=5$ and e) $N=40$. (Figure adapted with permissions from ref. [46]. Copyright: 2021, Wiley-VCH.)

sites to nearby area. For high RF electrodes, on the other hand, potential near HC sites would overlap, and some sites are in low potential region. As the directional LMT of OH⁻ is from high potential to low potential area, LMT of OH⁻ for sites located in low potential region would be suppressed and this causes a higher OH⁻ coverage as indicated in Figure 6e. This work implies that roughness of the electrode surface would influence LMT. High roughness catalysts lead to a weaken LMT as a result of the highly overlapped local electric field, suppress HER and enhance CORR selectivity.

The above roughness effect can be utilized to enhance the selectivity and activity of electrocatalytic reactions in many systems such as controlling the surface roughness of Cu catalysts for optimize the selectivity of CH₄, C₂H₄, or CO/HCOO—products in carbon-dioxide reduction reaction with suitable potential,^[67,68] preparing Au electrodes with high roughness factors to enhance CORR selectivity^[69] as well as electro-polishing Cu foil to optimize the roughness and the density of defect sites for high efficiency conversion of CO₂ to C₂+ products.^[70]

Besides of the above works described in detail, LMT has also been reported playing an important role in other systems. For example, Luo and his co-worker dispersed Pt-atom on curved carbon supports for efficient electrocatalytic hydrogen evolution, where a tip-enhancement effect at the Pt site extracting localized electrons from the support induces strong localized electric fields and further enhances the activity for HER.^[56]

Conclusion and Future Perspectives

In conclusion, we have reviewed the theoretical framework of nano-electrocatalysis as well as the impact of local-field-induced mass transfer (LMT) on several important systems. In the past decades, nanotechnology has been well developed, and nanocatalysts have been a common way of promoting the performance of electrocatalytic reactions. The rapid progress in nano-electrocatalytic experiments has brought and will bring plenty of interesting new findings. This is then a great opportunity to apply the theoretical framework of nano-electrocatalysis with LMT to unravel mysteries in complex nano-electrocatalytic systems. Future perspectives and challenges may be as follows. Firstly, this framework has proved to be successful in revealing the underlying mechanism in the systems we have reviewed. However, its application in other systems needs to be validated. Secondly, the concept of LMT might inspire new strategies to design nanocatalysts, which also need to be verified by further experiments. Additionally, the theoretical framework itself should be extended. For example, the electric potential near the surface is approximated by a given distribution form in the reviewed theoretical framework. To obtain better results for kinetics of nanocatalysis quantitatively, other methods such as the Poisson–Boltzmann equation which can give a more precise potential distribution should be coupled with this framework instead of the approximation form of the potential.^[71–73]

Acknowledgements

This work was supported by MOST(2018YFA0208702), the NSFC (32090044, 21973085, 21833007, 21790350, 21521001), Anhui Initiative in Quantum Information Technologies (AHY090200), and the Fundamental Research Funds for the Central Universities (WK2340000104).

Conflict of Interest

The authors declare no conflict of interest.

Keywords: electrochemistry · kinetics · local electric fields · mass transfer · nanocatalysis

- [1] Z. W. Seh, J. Kibsgaard, C. F. Dickens, I. Chorkendorff, J. K. Nørskov, T. F. Jaramillo, *Science* **2017**, *355*, eaad4998.
- [2] X. Tian, X. F. Lu, B. Y. Xia, X. W. Lou, *Joule* **2020**, *4*, 45–68.
- [3] S. Xu, E. A. Carter, *Chem. Rev.* **2019**, *119*, 6631–6669.
- [4] M. Cao, D. Wu, R. Cao, *ChemCatChem* **2014**, *6*, 26–45.
- [5] T. Zheng, K. Jiang, H. Wang, *Adv. Mater.* **2018**, *30*, e1802066.
- [6] O. S. Bushuyev, P. De Luna, C. T. Dinh, L. Tao, G. Saur, J. van de Lagemaat, S. O. Kelley, E. H. Sargent, *Joule* **2018**, *2*, 825–832.
- [7] D. Gao, R. M. Arán-Ais, H. S. Jeon, B. Roldan Cuenya, *Nat. Catal.* **2019**, *2*, 198–210.
- [8] A. Goyal, G. Marcandalli, V. A. Mints, M. T. M. Koper, *J. Am. Chem. Soc.* **2020**, *142*, 4154–4161.
- [9] M. B. Ross, P. De Luna, Y. Li, C.-T. Dinh, D. Kim, P. Yang, E. H. Sargent, *Nat. Catal.* **2019**, *2*, 648–658.
- [10] A. J. Bard, L. R. Faulkner, *Electrochemical Methods*, 2nd ed., Wiley, New York, **2001**.
- [11] A. Bruix, J. T. Margraf, M. Andersen, K. Reuter, *Nat. Catal.* **2019**, *2*, 659–670.
- [12] R. Zhou, Y. Zheng, M. Jaroniec, S.-Z. Qiao, *ACS Catal.* **2016**, *6*, 4720–4728.
- [13] N. Gupta, M. Gattrell, B. MacDougall, *J. Appl. Electrochem.* **2005**, *36*, 161–172.
- [14] R. Kas, R. Kortlever, H. Yilmaz, M. T. M. Koper, G. Mul, *ChemElectroChem* **2015**, *2*, 354–358.
- [15] D. Raciti, M. Mao, J. H. Park, C. Wang, *J. Electrochem. Soc.* **2018**, *165*, F799–F804.
- [16] N. A. Kotov, *Science* **2017**, *358*, 448.
- [17] H.-H. Li, M.-L. Xie, C.-H. Cui, D. He, M. Gong, J. Jiang, Y.-R. Zheng, G. Chen, Y. Lei, S.-H. Yu, *Chem. Mater.* **2016**, *28*, 8890–8898.
- [18] R. Qin, K. Liu, Q. Wu, N. Zheng, *Chem. Rev.* **2020**, *120*, 11810–11899.
- [19] J. Jiao, R. Lin, S. Liu, W. C. Cheong, C. Zhang, Z. Chen, Y. Pan, J. Tang, K. Wu, S. F. Hung, H. M. Chen, L. Zheng, Q. Lu, X. Yang, B. Xu, H. Xiao, J. Li, D. Wang, Q. Peng, C. Chen, Y. Li, *Nat. Chem.* **2019**, *11*, 222–228.
- [20] Y. Li, G. A. Somorjai, *Nano Lett.* **2010**, *10*, 2289–2295.
- [21] A. T. Bell, *Science* **2003**, 299.
- [22] Y. Sun, Y. Xia, *Science* **2002**, *298*, 2176.
- [23] Y. Xia, Y. Xiong, B. Lim, S. E. Skrabalak, *Angew. Chem. Int. Ed.* **2009**, *48*, 60–103; *Angew. Chem.* **2009**, *121*, 62–108.
- [24] C. Choi, S. Kwon, T. Cheng, M. Xu, P. Tieu, C. Lee, J. Cai, H. M. Lee, X. Pan, X. Duan, W. A. Goddard, Y. Huang, *Nat. Catal.* **2020**, *3*, 804–812.
- [25] C. P. Smith, H. S. White, *Anal. Chem.* **1993**, *65*, 3343–3353.
- [26] S. Chen, A. Kucernak, *J. Phys. Chem. B* **2002**, *106*, 9396–9404.
- [27] F. W. Campbell, R. G. Compton, *Anal. Bioanal. Chem.* **2010**, *396*, 241–259.
- [28] M. Lopez-Tenes, E. Laborda, A. Molina, R. G. Compton, *Anal. Chem.* **2019**, *91*, 6072–6079.
- [29] H. Le, C. Lin, E. Kätelhön, R. G. Compton, *Electrochim. Acta* **2019**, *298*, 778–787.
- [30] I. Streeter, R. G. Compton, *J. Phys. Chem. C* **2007**, *111*, 18049–18054.
- [31] J. J. Watkins, H. S. White, *Langmuir* **2004**, *20*, 5474–5483.
- [32] I. Streeter, R. Baron, R. G. Compton, *J. Phys. Chem. C* **2007**, *111*, 17008–17014.
- [33] C. Lin, R. G. Compton, *J. Phys. Chem. C* **2017**, *121*, 2521–2528.
- [34] C. Lin, R. G. Compton, *Curr. Opin. Electrochem.* **2019**, *14*, 186–199.

- [35] S. Chen, Y. Liu, *Phys. Chem. Chem. Phys.* **2014**, *16*, 635–652.
- [36] S. W. Feldberg, *Anal. Chem.* **2010**, *82*, 5176–5183.
- [37] M. C. Henstridge, E. Laborda, R. G. Compton, *J. Electroanal. Chem.* **2012**, *674*, 90–96.
- [38] M. C. Henstridge, E. Laborda, Y. Wang, D. Suwatchara, N. Rees, Á. Molina, F. Martínez-Ortiz, R. G. Compton, *J. Electroanal. Chem.* **2012**, *672*, 45–52.
- [39] M. C. Henstridge, K. R. Ward, R. G. Compton, *J. Electroanal. Chem.* **2014**, *712*, 14–18.
- [40] M. C. Henstridge, R. G. Compton, *Chem. Rec.* **2012**, *12*, 63–71.
- [41] S. Chen, Y. Liu, J. Chen, *Chem. Soc. Rev.* **2014**, *43*, 5372–5386.
- [42] R. B. Schoch, J. Han, P. Renaud, *Rev. Mod. Phys.* **2008**, *80*, 839–883.
- [43] H. Jiang, Z. Hou, Y. Luo, *Angew. Chem. Int. Ed.* **2017**, *56*, 15617–15621; *Angew. Chem.* **2017**, *129*, 15823–15827.
- [44] Q. X. Chen, Y. H. Liu, X. Z. Qi, J. W. Liu, H. J. Jiang, J. L. Wang, Z. He, X. F. Ren, Z. H. Hou, S. H. Yu, *J. Am. Chem. Soc.* **2019**, *141*, 10729–10735.
- [45] Q. X. Chen, Y. H. Liu, Z. He, J. L. Wang, J. W. Liu, H. J. Jiang, W. R. Huang, G. Y. Gao, Z. H. Hou, S. H. Yu, *J. Am. Chem. Soc.* **2021**, *143*, 32, 12600–12608.
- [46] Y. Liu, H. Jiang, Z. Hou, *Angew. Chem. Int. Ed.* **2021**, *60*, 11133–11137.
- [47] M. Liu, Y. Pang, B. Zhang, P. De Luna, O. Voznyy, J. Xu, X. Zheng, C. T. Dinh, F. Fan, C. Cao, F. P. de Arquer, T. S. Safaei, A. Mepham, A. Klinkova, E. Kumacheva, T. Filleter, D. Sinton, S. O. Kelley, E. H. Sargent, *Nature* **2016**, *537*, 382–386.
- [48] T. Saberi Safaei, A. Mepham, X. Zheng, Y. Pang, C. T. Dinh, M. Liu, D. Sinton, S. O. Kelley, E. H. Sargent, *Nano Lett.* **2016**, *16*, 7224–7228.
- [49] F.-Y. Gao, R.-C. Bao, M.-R. Gao, S.-H. Yu, *J. Mater. Chem. A* **2020**, *8*, 15458–15478.
- [50] M. Li, S. Garg, X. Chang, L. Ge, L. Li, M. Konarova, T. E. Rufford, V. Rudolph, G. Wang, *Small Methods* **2020**, *4*.
- [51] Y. H. Li, P. F. Liu, C. Li, H. G. Yang, *Chem. Eur. J.* **2018**, *24*, 15486–15490.
- [52] C. Chen, Y. Pang, F. Zhang, J. Zhong, B. Zhang, Z. Cheng, *J. Mater. Chem. A* **2018**, *6*, 19621–19630.
- [53] F. Y. Gao, S. J. Hu, X. L. Zhang, Y. R. Zheng, H. J. Wang, Z. Z. Niu, P. P. Yang, R. C. Bao, T. Ma, Z. Dang, Y. Guan, X. S. Zheng, X. Zheng, J. F. Zhu, M. R. Gao, S. H. Yu, *Angew. Chem. Int. Ed.* **2020**, *59*, 8706–8712; *Angew. Chem.* **2020**, *132*, 8784–8790.
- [54] C. Jia, Y. Zhang, X. Wang, W. Zhong, O. V. Prezhdo, Y. Luo, J. Jiang, *J. Mater. Chem. A* **2020**, *8*, 12485–12494.
- [55] P. An, L. Wei, H. Li, B. Yang, K. Liu, J. Fu, H. Li, H. Liu, J. Hu, Y.-R. Lu, H. Pan, T.-S. Chan, N. Zhang, M. Liu, *J. Mater. Chem. A* **2020**, *8*, 15936–15941.
- [56] D. Liu, X. Li, S. Chen, H. Yan, C. Wang, C. Wu, Y. A. Haleem, S. Duan, J. Lu, B. Ge, P. M. Ajayan, Y. Luo, J. Jiang, L. Song, *Nat. Energy* **2019**, *4*, 512–518.
- [57] J. Li, S. Chen, F. Quan, G. Zhan, F. Jia, Z. Ai, L. Zhang, *Chem* **2020**, *6*, 885–901.
- [58] W. Liu, S. W. Lee, D. Lin, F. Shi, S. Wang, A. D. Sendek, Y. Cui, *Nat. Energy* **2017**, *2*.
- [59] X. Mao, P. Brown, C. Cervinka, G. Hazell, H. Li, Y. Ren, D. Chen, R. Atkin, J. Eastoe, I. Grillo, A. A. H. Padua, M. F. Costa Gomes, T. A. Hutton, *Nat. Mater.* **2019**, *18*, 1350–1357.
- [60] W. Cheng, X. Teng, C. Lu, *Anal. Chem.* **2020**, *92*, 5456–5463.
- [61] W. Jiao, C. Chen, W. You, X. Zhao, J. Zhang, Y. Feng, P. Wang, R. Che, *Adv. Energy Mater.* **2020**, *10*, 1904072.
- [62] O. Jahanmahin, D. J. Kirby, B. D. Smith, C. A. Albright, Z. A. Gobert, C. D. Keating, K. A. Fichthorn, *J. Phys. Chem. C* **2020**, *124*, 9559–9571.
- [63] L. Li, T. Yang, K. Wang, H. Fan, C. Hou, Q. Zhang, Y. Li, H. Yu, H. Wang, *J. Colloid Interface Sci.* **2021**, *583*, 188–195.
- [64] Q.-X. Chen, S.-H. Yu, *Trends Chem.* **2020**, *2*, 888–897.
- [65] Y. Ren, Y. Zou, Y. Liu, X. Zhou, J. Ma, D. Zhao, G. Wei, Y. Ai, S. Xi, Y. Deng, *Nat. Mater.* **2020**, *19*, 203–211.
- [66] L. Wang, S. Nitopi, A. B. Wong, J. L. Snider, A. C. Nielander, C. G. Morales-Guio, M. Orazov, D. C. Higgins, C. Hahn, T. F. Jaramillo, *Nat. Catal.* **2019**, *2*, 702–708.
- [67] K. Jiang, Y. Huang, G. Zeng, F. M. Toma, W. A. Goddard, A. T. Bell, *ACS Energy Lett.* **2020**, *5*, 1206–1214.
- [68] D. Ren, J. Fong, B. S. Yeo, *Nat. Commun.* **2018**, *9*, 925.
- [69] B. A. Zhang, T. Ozel, J. S. Elias, C. Costentin, D. G. Nocera, *ACS Cent. Sci.* **2019**, *5*, 1097–1105.
- [70] T. Kim, G. T. R. Palmore, *Nat. Commun.* **2020**, *11*, 3622.
- [71] K. B. Oldham, A. M. Bond, *J. Electroanal. Chem.* **2001**, *508*, 28–40.
- [72] R. He, S. Chen, F. Yang, B. Wu, *J. Phys. Chem. B* **2006**, *110*, 3262–3270.
- [73] E. J. F. Dickinson, R. G. Compton, *J. Electroanal. Chem.* **2011**, *661*, 198–212.

Manuscript received: July 29, 2021

Accepted manuscript online: September 21, 2021

Version of record online: October 14, 2021